The Astrophysical Journal, 802:31 (8pp), 2015 March 20 doi:10.1088/0004-637X/802/1/31

A PROTOCLUSTER AT $z = 2.45$

C. Diener[1,2], S. J. Lilly[1], C. Ledoux[2], G. Zamorani[3], M. Bolzonella[3], D. N. A. Murphy[4], P. Capak[5], O. Ilbert[6], and H. McCracken[7]

[1] Institute for Astronomy, Department of Physics, ETH Zurich, Zurich 8093, Switzerland; cdiener@phys.ethz.ch
[2] European Southern Observatory, Alonso de Córdova 3107, Casilla 19001, Vitacura, Santiago, Chile
[3] INAF, Osservatorio Astronomico di Bologna, Via Ranzani 1, I-40127, Bologna, Italy
[4] Instituto de Astrofísica, Facultad de Física, Pontificia Universidad Católica de Chile, Av. Vicuña Mackenna 4860, 782–0436 Macul, Santiago, Chile
[5] Spitzer Science Center, 314–6 Caltech, Pasadena, CA 91125, USA
[6] Aix Marseille Université, CNRS, LAM (Laboratoire d'Astrophysique de Marseille) UMR 7326, F-13388, Marseille, France
[7] Institut d'Astrophysique de Paris, UMR 7095 CNRS, Université Pierre et Marie Curie, Paris, France
Received 2014 November 3; accepted 2014 December 29; published 2015 March 18

ABSTRACT

We present the spectroscopic confirmation of a $z = 2.45$ protocluster. Its member galaxies lie within a radius of 1.4 Mpc (physical) on the sky and within $\Delta v \pm 700$ km s^{-1} along the line of sight. We estimate an overdensity of 10, suggesting that the structure has made the turnaround but is not assembled yet. A comparison to the Millennium simulation suggests that analogous structures evolve into 10^{14}–10^{15} $M_{\odot}\,h^{-1}$ type dark matter halos by $z = 0$, qualifying the notion of "protocluster." The search for the complete census of mock progenitor galaxies at $z \sim 2.5$ of these massive $z = 0$ mock clusters reveals that they are widely spread over areas with a diameter of 3–20 Mpc. This suggests that the optical selection of such protoclusters can result in a rich diversity regarding their $z = 0$ descendants. We also searched for signs of environmental differentiation in this protocluster. While we see a weak trend for more massive and more quiescent galaxies within the protocluster, this is not statistically significant.

Key words: galaxies: clusters: general – galaxies: high-redshift

1. INTRODUCTION

The identification of galaxy groups and clusters in the high-redshift universe may offer insights into both the formation of structure in the universe and the evolution of individual galaxies. The study of the most massive structures at a given epoch serves as a laboratory for cosmology. It is also known that, at least at later epochs, $z < 1$, the cluster or group environment can influence the member galaxies through a variety of processes. The existence of a morphology–density relation has been established, stating that denser environments host a higher fraction of morphological types that are typically associated with a lower star formation rate (Oemler 1974; Dressler 1980; Balogh et al. 2004; Wuyts et al. 2011). Furthermore, the fraction of galaxies that are "quenched," i.e., in which star formation has ceased or has been suppressed to yield a specific star formation rate that is below the inverse Hubble time, is higher in high-density environments and among satellite galaxies relative to central galaxies at the same mass (e.g., Peng et al. 2010, 2012; Knobel et al. 2013; Wetzel et al. 2013; Kovač et al. 2014; Koyama et al. 2014). A variety of effects such as ram pressure stripping (Gunn & Gott 1972; Dressler 1980; Abadi et al. 1999), strangulation (Larson et al. 1980; Kawata & Mulchaey 2008), harassment (Moore et al. 1996), and so on have been invoked as causes of the suppression of star formation in satellites.

The terminology of the membership of forming structures at high redshift should be carefully defined. Following Diener et al. (2013), when we refer to an association of galaxies as a cluster (or group), we mean that its member galaxies occupy the same dark matter (DM) halo at the time we observe it. This effectively means that the galaxies lie within the r_{200} perimeter of a single DM halo. Of course, this perimeter cannot be observed directly in the sky, and so reliance must be made on comparison with mock catalogs of galaxies that have been generated from large-scale numerical simulations like the Millennium simulation (Springel et al. 2005; Kitzbichler & White 2007; Henriques et al. 2012). In contrast, the member galaxies of a protocluster (or protogroup) occupy different DM halos at the epoch at which they are being observed, but they will later accrete into a common halo by $z = 0$. The galaxy members of a protogroup are therefore mostly still the dominant galaxies in their individual DM halos (i.e., are "centrals"), but they will later become "satellites" in the larger structure.

In a similar manner to group or cluster identification via mock catalogs, protoclusters can also be identified in simulations (Diener et al. 2013 and this work). Furthermore, simulations can be used to follow the evolution of a protocluster and predict its "product" at any later cosmic time. In turn, this approach also provides information about the progenitors of today's clusters.

Whereas the aforementioned environmental processes take place and have been observed in assembled groups and clusters at $z < 1$, it is still unclear at which stage of the evolution of a protocluster to a cluster the onset of environmental differentiation happens.

It is clear that, at a given stellar mass, the properties of satellites in the local universe are systematically different from those of typical centrals (see, e.g., van den Bosch et al. 2008; Weinmann et al. 2009; Pasquali et al. 2010; Peng et al. 2012). This environmental central–satellite differentiation has been established out to $z \sim 1$ (Gerke et al. 2007; Knobel et al. 2013; Kovač et al. 2014). If the environmental effects in the galaxy population are dominated by satellites (see Knobel et al. 2014 for a qualification of this), then it is possible that at $z \sim 2$ the members of a protogroup or protocluster would not be environmentally differentiated from the general population because these galaxies will (by definition) still be centrals and not satellites. Whether this is true is, however, not clear yet, and

a $z < 1$ relation does not necessarily hold at $z > 2$. Also, environmental differentiation (even among centrals) could enter in new ways at high redshifts. It is clear in the continuity approach of Peng et al. (2010) that quenched galaxies first appear as the characteristic M^* of galaxies (and halos) approaches the mass scale at which quenching occurs, which appears to be more or less constant with redshift (Peng et al. 2010; Behroozi et al. 2013). As these galaxies quench, the galaxy mass function decouples from the halo mass function and subsequently evolves "vertically" (with increasing ϕ^* but more or less constant M^*). Lilly et al. (2013) referred to this transition as that between phase 1 and phase 2 of the evolution of the galaxy population. Seen another way, the relative numbers of quenched and star-forming galaxies around the galaxy stellar M^* reflect the slope of the halo mass function at and above this quenching mass (see the discussion in Birrer et al. 2014). At high redshift, the halo mass function has a Schechter M^* that is much closer to this quenching mass than it is at low redshifts, where the DM M^* is of course much larger. Differences in the halo mass function in different large-scale environments may then lead to significant environmental differentiation among the population of centrals, quite independent of those astrophysical effects on the group or cluster members that appear to dominate at lower redshifts.

The literature to date shows at times contradictory examples for environmental influences in protoclusters at $z > 2$. Kodama et al. (2007) detect a well-populated emerging red sequence in three $z > 2$ protoclusters, suggesting the appearance of massive elliptical galaxies, whereas Hatch et al. (2011) only see a poorly populated red sequence in their sample of six protoclusters at $z \sim 2.4$. Furthermore, Hatch et al. (2011) find evidence that protocluster members are both about twice as massive and have lower specific star formation rates than the field galaxies at the same redshift. A similar, tentative result was found by Lemaux et al. (2014) in a $z = 3.3$ protocluster. Shimakawa et al. (2014), on the other hand, report increased star formation in two $z > 2$ protoclusters. In our previous work (Diener et al. 2013), we studied lower-mass structures than those mentioned above and did not find any evidence for environmental differentiation. The same result is also found by Cucciati et al. (2014) at slightly higher redshift ($z = 2.9$). While these different results may have their roots in a variety of causes (such as different halo masses), it is also possible that the cause is the protocluster selection (e.g., Hα emitters versus optical selection or selection criteria applied) made by these authors.

In this work we present a $z = 2.45$ protocluster (Section 2) that we have identified in a follow-up of a number of protogroup structures originally identified in the zCOSMOS-deep survey (S. J. Lilly et al. 2015, in preparation) by Diener et al. (2013). The layout of this paper is as follows. We first describe in Section 2 the follow-up spectroscopic observations that led to the confirmation of the $z = 2.45$ protocluster. We then compare the distribution of the members of this structure with simulations in Section 3, in order to establish at which stage of the process of cluster assembly it is and to predict its evolution to $z = 0$. In Section 4, we then examine its galaxy population in a search for any differences from the field population at the same redshift. We summarize our results and draw conclusions in Section 5.

All magnitudes are quoted in the AB system, and we use the ΛCDM cosmology with $\Omega_m = 0.25$, $\Omega_\Lambda = 0.75$, and $H_0 = 73$ km s^{-1} Mpc^{-1}, in line with the parameters used for the Millennium simulation. We refer to physical (comoving) distances with a prefix "p" ("c"); for example, pMpc would correspond to physical megaparsecs.

2. DATA

2.1. zCOSMOS-deep and the Protogroup Catalog

The zCOSMOS-deep sample (Lilly et al. 2007; S. J. Lilly et al. 2015, in preparation) provides around ~3500 spectroscopic redshifts at $2 < z < 3$, observed with the VLT/VIMOS low-resolution LR-Blue grism. This instrument configuration yields a spectral resolution of $R = 180$ and a spectral range of 3700–6700 Å. The zCOSMOS-deep targets lie in the central field of COSMOS, covering in total a region of $0.^{\circ}92 \times 0.^{\circ}91$, centered on 10 00 43 (R.A.), 02 10 23 (decl.), with a denser sampled inner area of $0.^{\circ}60 \times 0.^{\circ}62$. The targets were selected with a combination of *BzK* and *ugr* selection (see Daddi et al. 2004; Steidel et al. 2004). All targets have $B_{AB} < 25.25$, and the *BzK*-selected galaxies also fulfill $K_{AB} < 23.5$. The zCOSMOS-deep survey has a sampling rate of close to 50%, consisting of a spatial sampling rate of 67% and a success rate in assigning redshift of 60% (see S. J. Lilly et al. 2015, in preparation, for details).

In our previous paper (Diener et al. 2013), we identified 42 candidate protogroups at $1.8 < z < 3$ in the zCOSMOS-deep sample, using a friends-of-friends (FOF) approach with linking lengths $dr = 500$ kpc and $dv = 700$ km s^{-1}. These protogroups have three to five members and, as argued in that paper, are not likely to already be assembled at the epoch of observation, but the vast majority of them will assemble by $z = 0$. We selected seven of these spectroscopically identified protogroups for follow-up spectroscopy to confirm the previous member galaxies and to identify additional members.

2.2. FORS2 Data

The VLT/FORS2 spectroscopy was taken in 2011 March, using the instrument in its MXU mode with the E2V CCD being sensitive in the blue (<5000 Å) and the 300 V grism. We observed a total of five multislit masks and obtained spectra for 114 $z_{\rm phot} \gtrsim 2$ galaxies in five $6.'8 \times 6.'8$ regions (at times overlapping). The protocluster we present in this work was covered by three of the five masks. Two of these were observed for 5.5 hr and the remaining for 6 hr under good seeing conditions ($0.''8$–$1.''0$).

The targets for the observations were selected from the COSMOS photo-z sample (Capak et al. 2007; Ilbert et al. 2009) as follows:

1. They had to lie in the surroundings (within 2 Mpc physical) of the already spectroscopically confirmed protogroups.
2. Their photo-z had to be consistent with the respective protogroup redshift (i.e., with a $\Delta v < 20{,}000$ km s^{-1}).
3. The targets had to fulfill $B_{AB} < 25.5$ or IRAC 3.6 μm < 22 (or both).

These new targets were supplemented by the already spectroscopically confirmed members from zCOSMOS-deep, in order to confirm their redshifts and obtain more accurate relative velocities with the higher resolution of FORS2 in comparison to VIMOS.

Table 1
The 11 Spectroscopically Confirmed Members of the Protocluster Presented in This Work.

ID	R.A.	Decl.	z_{spec}	r_i (kpc)	v_i (km s^{-1})
429950	149.996613	2.256573	2.442	463	−369
429868	150.007828	2.249362	2.443	321	−256
410000	150.008743	2.264080	2.442	713	−322
409614	149.995026	2.239803	2.439	167	−565
1029209	149.975500	.227124	2.440	846	−530
1034036	149.99157	2.194295	2.451	1409	414
1031108	149.97563	2.21506	2.446	1064	−17
1023628	150.01885	2.265366	2.446	891	31
1023927	150.01939	2.261413	2.450	812	361
1032336	149.98813	2.206609	2.453	1085	655
1022028	150.02802	2.274885	2.453	1278	598

Note. We list their identifier (ID), R.A., dec1., redshift, radial distance (r_i), and velocity along the line of sight v_i with respect to the protocluster center defined by mean R.A. (150.00048), dec1. (2.24132), and z

The data were reduced in the standard way with the IRAF apextract package, and the redshifts were determined through a visual inspection of the individual spectra. Of the 114 targets, we were able to assign spectroscopic redshifts to 67 objects (or 60%). The success rate in assigning redshifts was dependent on observing conditions and integration time. Because the masks covering the area of interest in this paper had both the best conditions and highest integration times (5.5 and 6 hr), the actual success rate in that area is as high as 71%.

2.3. Protocluster at $z = 2.45$

We detected a large structure with a total of 11[8] spectroscopically confirmed members at a mean redshift of $z = 2.45$, R.A. = 150.00, and dec1. = 2.24 in the FORS2 data. A list of the members is given in Table 1. The 11 members of this structure all lie within a 1.4 Mpc radius (physical) on the sky and within a velocity range Δv of ± 700 km s^{-1}.

We calculated the rms radial size $r_{\rm rms}$ and velocity spread $v_{\rm rms}$ to be $r_{\rm rms} = \sqrt{\sum_i r_i^2/(N-1)} = 902$ kpc and $v_{\rm rms} = \sqrt{\sum_i v_i^2/(N-1)} = 426$ km s^{-1}, where r_i and v_i indicate the distance and the velocity of a galaxy relative to the mean, and N is the number of galaxies. As we will argue in Sections 3.1 and 4.1, this structure is probably not yet gravitationally bound, and so these values should not be used to infer a virial mass of the structure.

The spatial distribution of member galaxies is shown in Figure 1.

2.4. The Mock Sample

In order to learn about the likely nature of the underlying dark matter structure of this protocluster, we need mock catalogs generated to resemble as accurately as possible the observational situation. For this purpose we make use of the Millennium simulation (Springel et al. 2005) and light cones from Henriques et al. (2012). Through the identification of similar structures in these mock samples, where full DM and evolutionary information is available, we get indications about the nature and evolution of the observed structure.

2.4.1. The Millennium Simulation and Henriques Light Cones

The Millennium simulation followed the DM distribution in a cubic box of 500 Mpc h^{-1} side length starting at $z = 127$ and following the evolution of the DM particles through time down to $z = 0$. As the results are stored in only 64 snapshots, the DM structure and its merger trees are built up in postprocessing (Springel et al. 2005; Lemson et al. 2006). The identified halos are populated with galaxies whose evolution is described by a semianalytic model (SAM).

Henriques et al. (2012) construct their light cones from the Millennium simulation volume with the implementation of the SAM described in Guo et al. (2011). They follow the description by Kitzbichler & White (2007) for periodic replication of the simulation box needed to achieve cones that cover a wide redshift range and assign galaxy redshifts according to the comoving distance of galaxies to a $z = 0$ virtual observer. The resulting 24 light cones cover an area of 1.4×1.4 deg^2 each.

2.4.2. Construction of Mock Samples

The targets for the FORS2 observations were selected from a photo-z sample but were chosen to be at the position of known overdensities from the initial spectroscopic zCOSMOS sample. In attempting to mimic this situation as accurately as possible, we chose a two-stage approach in constructing the mock sample.

First we created mock samples that were intended to replicate the zCOSMOS-deep sample from which we draw our original candidate group. In this we followed the prescription in Diener et al. (2013), using magnitude cuts on the mock galaxies to achieve number densities in the mocks that match those in the spectroscopic sample. The roughly 50% sampling of zCOSMOS-deep allows us to construct two mock catalogs from each light cone, resulting in 48 zCOSMOS-deep mock catalogs. Because the protocluster in question was originally identified with five zCOSMOS-deep galaxies, we next constructed a mock group catalog from these zCOSMOS mock samples by applying the same group-finding criteria as for the original candidate group; that is, we applied an FOF algorithm with linking lengths $dr = 500$ kpc and $dv = 700$ km s^{-1} and restricted ourselves to protogroups with five members.

In a second stage, we aimed to reproduce the subsequent FORS2 observations by first creating a mock target sample from the light cones that resembles the underlying COSMOS photo-z sample from which the targets were selected. As mentioned above, the objects in our target catalog had to fulfill $B_{AB} < 25.5$ and/or IRAC 3.6 μm < 22, as well as having a photo-z consistent with the respective previously identified group. We applied a photo-z error of 10,000 km s^{-1} (this corresponds to the typical observed photo-z error at $z \sim 2.5$) to the mock redshifts and cut the mock sample in B and IRAC 3.6 μm. These cuts where adjusted such that the number density of our target catalog from COSMOS matched the mock sample. From this mock target catalog we then randomly drew 16% of all objects to mimic the product of the fraction of targets actually observed (22%) and the success rate in

[8] With seven targeted protogroups and 114 observed objects, we observed ~16 candidate members per protogroup. All protogroups were confirmed, some with one or two additional members. The protocluster presented in this work is by far the most extreme structure we found. The overall low rate of additional members is due to the high photo-z uncertainties.

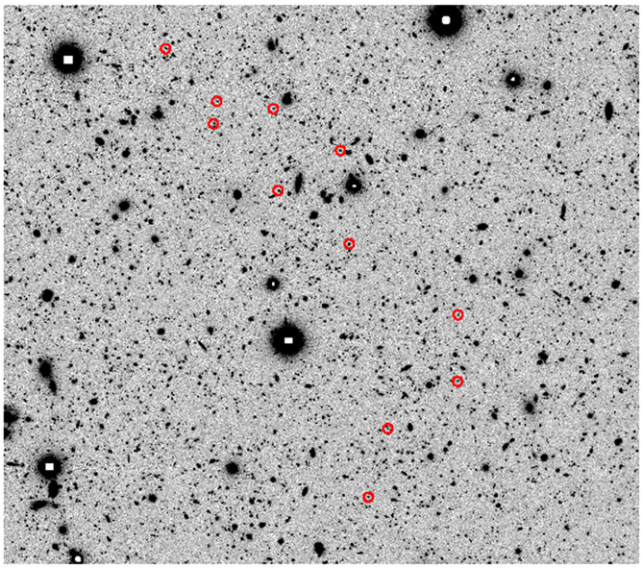

Figure 1. The 11 members of the protocluster (red circles) in a Subaru *B*-band image. They lie within a radius of 1.4 Mpc (physical, corresponding to 2.9).

assigning redshift (71%). We populated the already-existing group catalog with this "observed" sample.

In the final sample we searched for protoclusters that had 11 or more members lying within 1.4 Mpc and 700 km s^{-1} (same as the FORS2 protocluster). This resulted in 16 candidate protoclusters in the redshift range $2.3 < z < 2.6$, distributed over the 48 mock samples of 2 deg^2 each.

3. EVOLUTION IN SIMULATIONS

3.1. Surface Number Densities

As mentioned above, with our selection technique, we detect 16 candidate protoclusters in the 96 deg^2 of the 48 mock samples, or 0.17 protoclusters per deg^2. In other words, we expect one such system in the $z \sim 2.5$ redshift range in a 6 deg^2 field. Based on this, finding one in the region of zCOSMOS-deep (1 deg^2 in total and 0.36 deg^2 in the area of maximum coverage) appears lucky, but not exceptionally so.

3.2. Assembly History

While at low redshift galaxy clusters will usually have mostly assembled (i.e., have their member galaxies occupying the same DM halo) and will in many cases be virialized, this is not the case at $z > 2$. The growth of structure is so rapid at these masses at high redshift that even quite substantial overdensities will most likely be at a "preassembly" stage, meaning that their member galaxies will accrete onto a common DM halo by $z = 0$ but are still occupying different halos when they are being observed (e.g., Diener et al. 2013). We refer to these forming structures as "protogroups" or "protoclusters."

We can use the properties of the structures in the mock catalogs to infer the likely state of the system we see in the sky. In the case of the 16 protoclusters in the mock sample, the majority (10 or 62.5%) have already started assembly at $z \sim 2.5$, in the sense that the largest halo already contains between two and four galaxies that meet our selection criteria (note that there may also be fainter galaxies residing in the same halos). About a third of the $z \sim 2.5$ protoclusters,

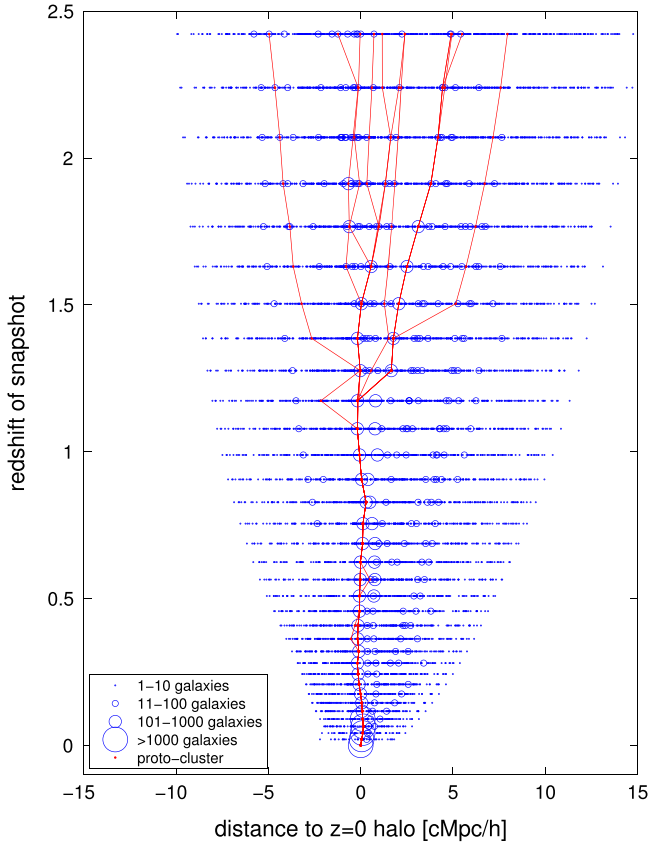

Figure 2. The assembly history of a $z \sim 2.5$ protocluster. We follow all halos that will eventually become part of the same $z = 0$ DM halo, i.e., form a cluster. The size of the circles corresponds to the number of galaxies that inhabit a given halo. While at $z \sim 2.5$ galaxies are mostly centrals themselves, they continuously accrete onto other halos to eventually become satellites in the $z = 0$ cluster. The protocluster member halos we identify at $z \sim 2.5$ are highlighted in red.

however, still consist entirely of singletons. The assembly process continues to $z = 0$ when 13 (81%) have fully assembled (i.e., with all of the detected members within a common halo) or mostly assembled (i.e., more than 50% of its members in a common halo). Only for three (19%) of the mock clusters is the contamination by interlopers high enough that less than 50% of the identified members end up occupying the same halo at $z = 0$.

We illustrate the assembly of such a protocluster in Figure 2, by following the halos of all galaxies from $z \sim 2.5$ that will eventually become members of the same $z = 0$ cluster. We highlight the protocluster galaxies that we identified in our mock catalog in red, but obviously many more galaxies are part of this massive $z = 0$ cluster, and at $z \sim 2.5$ they are distributed over rather large scales (see Section 3.4 for further discussion). Also evident from this figure is that the originally identified protocluster members largely complete their accretion process before $z = 1$, consistent with the idea that the structure has made its turnaround (see Section 4.2).

Overall, on average, in the mock catalogs, 78% of the identified protocluster members will end up being true cluster members by the present epoch, whereas only 16% are already in the same halo at $z \sim 2.5$. These numbers suggest that the presented structure is a true protocluster in the sense that the vast majority of the galaxies will end up in a massive (see next section) cluster today, but only a small minority are already

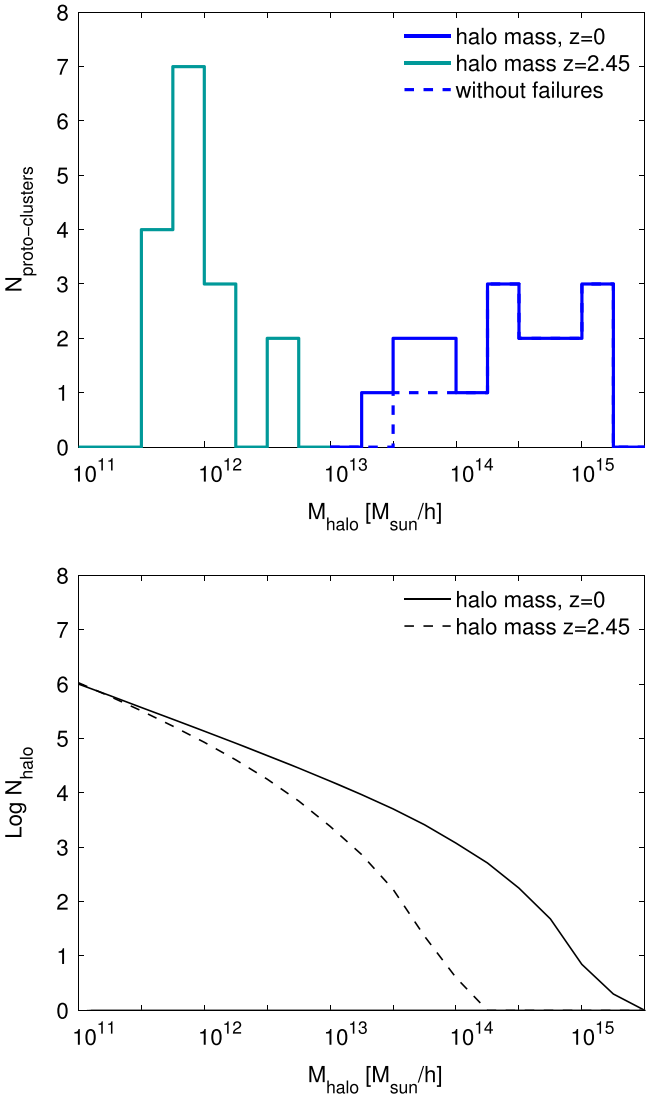

Figure 3. Top panel: halo masses of the most massive halo of the mock protoclusters at $z = 2.45$ (turquoise) and at $z = 0$ (blue). While evolving from a rather unremarkable halo ($\sim 10^{12}\ M_{\odot}\ h^{-1}$), they will become some of the most massive clusters by $z = 0$ with a halo mass of $\sim 5 \times 10^{14}\ M_{\odot}\ h^{-1}$. The dashed line indicates the halo masses without the three clusters that do not assemble, i.e., that end with <50% of the members in the same halo. Bottom panel: halo mass functions at $z = 2.45$ (dotted) and $z = 0$ (solid) for comparison.

sharing the same DM halo at the high redshift at which we observe them.

3.3. Halo Masses

As established in the previous section, the member galaxies of the protocluster are not likely to occupy the same DM halo at $z \sim 2.5$. However, it is illustrative to compare the typical halo at $z \sim 2.5$ to the fully evolved cluster halo at $z = 0$ by following the evolution of these halos in the simulation. At $z \sim 2.5$ the protocluster galaxies reside in somewhat unremarkable halos with masses of $\sim 10^{12}\ M_{\odot}\ h^{-1}$, simply because they are mostly singleton galaxies. This changes dramatically by $z = 0$, when the former protocluster members mostly inhabit halos with $M_{\rm halo} = 10^{14} - 10^{15}\ M_{\odot}\ h^{-1}$; that is, they become members of the most massive clusters seen today. This is illustrated in Figure 3, where we show the distribution of halo masses of the protocluster at $z \sim 2.5$ and $z = 0$ (top panel), as well as the halo mass functions at both redshifts for comparison (bottom panel). This again underlines the use of the terminology "protocluster." At $z \sim 2.5$ this structure is an assembly of galaxies residing as centrals in their DM halo. As it evolves, these halos merge to eventually form a massive cluster halo that is occupied by the previously identified centrals and by galaxies that accreted later on or were below the detection limit at $z \sim 2.5$.

3.4. Progenitor Galaxies

We established in the previous section that the mock protoclusters evolve into very massive $z = 0$ clusters. This suggests that other progenitor galaxies to these clusters exist, in addition to the ~11 identified members. All of these progenitors will become part of the same DM halo by $z = 0$. They could have failed to be identified as members of the protocluster for a variety of reasons. First of all, the spectroscopy was restricted to relatively bright ($B_{AB} < 25.5$) targets. The objects that met the selection criterion have been sampled incompletely, due to both a limited spatial sampling[9] and a <100% success rate in assigning redshifts.

We searched for the additional $z \sim 2.5$ progenitors in the light cones, with the result shown in Figure 4. The progenitors are color and size coded according to their B-band magnitude, showing the very faint objects in green and the brightest in dark blue. There are a significant number of such progenitors present in each of the protocluster fields (median of 2215; the $z = 0$ cluster will have fewer members than that as some progenitor galaxies merge), but most of them are too faint to have met our selection criterion. The vast majority (95%) of these objects, however, meet the $\Delta v < 700\ {\rm km\ s^{-1}}$ condition that would associate them with the protocluster if observed.

The diameter of the area occupied by progenitors ranges from 3 pMpc to 20 pMpc. This range of areas is also reflected in the range of halo masses (Figure 3), which occupy almost two orders of magnitude. Only as the cluster assembles does it turn into the more compact structure observed at lower redshifts. The optical selection of such a protocluster can hence result in a diversity of objects. This analysis also hints at a more extended structure at $z = 2.45$ in the COSMOS field. As the range 3–20 pMpc corresponds to an angular scale of 6′–41′, comparable to or bigger than the FORS2 FOV (6.′8 × 6.′8), we would not have detected this extended structure with our observations.

4. OBSERVATIONAL CHARACTERISTICS

According to simulations, the $z = 2.45$ protocluster is likely to evolve into a massive cluster by $z = 0$, but it is only just starting its assembly. While this implies that the effects that shape the group population at $z < 1$ cannot take place yet, the overdense environment of a protocluster could influence the member galaxies and hence make them distinguishable from the field galaxies at the same redshift.

4.1. Photo-z Samples

The selection of galaxies in zCOSMOS-deep and also for the FORS2 observation involved a cut in the B magnitude. The spectroscopic sample is therefore highly incomplete in mass

[9] The FORS2 observations only allowed ~20–25 objects per mask.

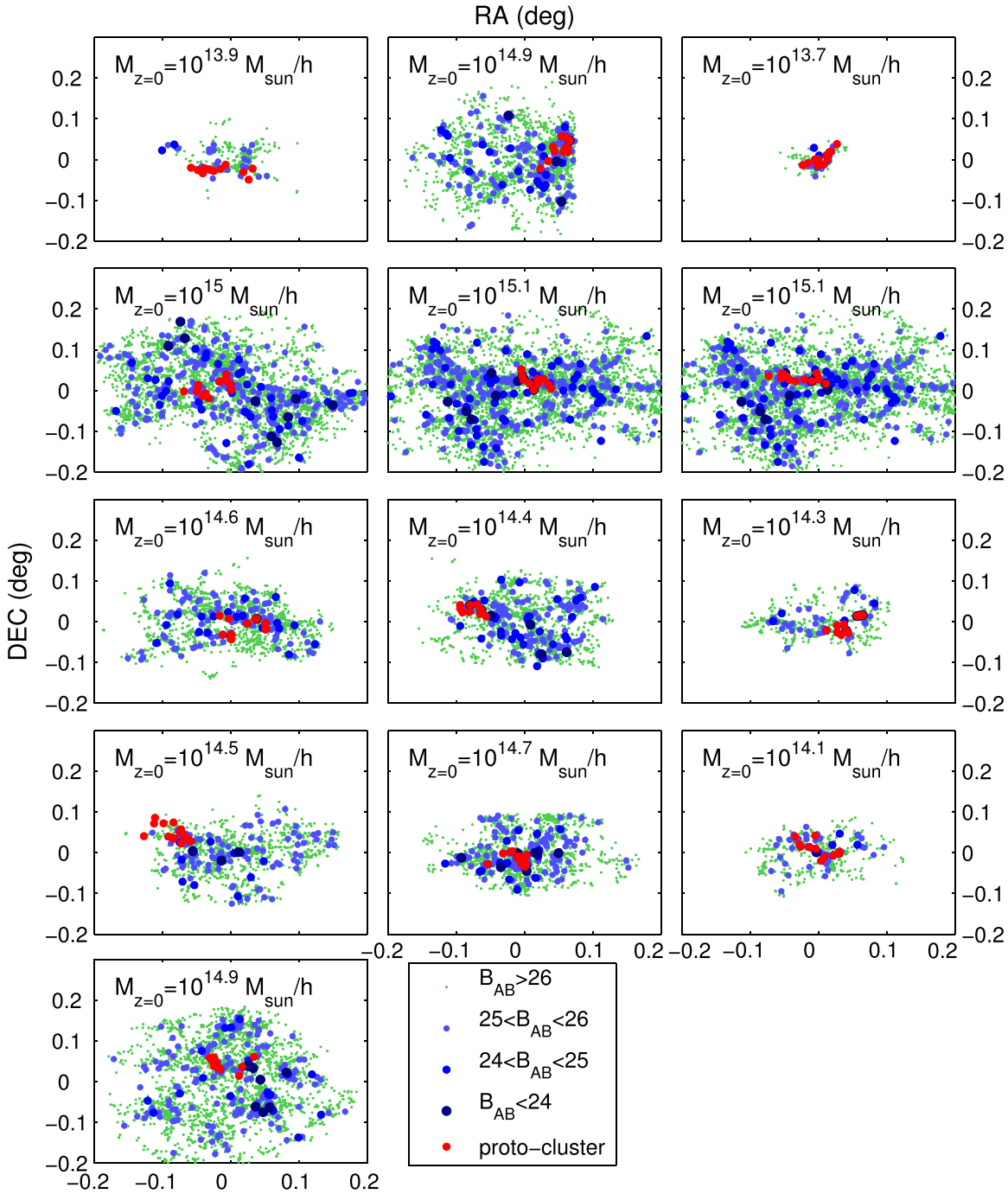

Figure 4. All $z \sim 2.5$ progenitor galaxies (green and blue) that will by $z = 0$ become members of the cluster that we identified by our protocluster selection. The actual protocluster members that identify the structure are highlighted in red. In each protocluster field there exist several hundred to thousands of progenitors, most of them too faint for observations. We also note the $z = 0$ halo mass that reflects the number of progenitors. Two of the $z = 0$ clusters are identical: their progenitor hosts so many galaxies that they were detected in both of the depleted mock catalogs (we randomly split the original catalog into two parts to mimic the spectroscopic sampling rate of zCOSMOS-deep).

and will be biased against red objects that are quiescent or that have high reddening. Any interesting statements about the population of galaxies in the protocluster region compared with those in the surrounding "field" must therefore be based on photo-z sample(s), despite the high-redshift uncertainties therein.

To that end, we use two photo-z samples, one being the i-band selected photo-z catalog from Capak et al. (2007) and Ilbert et al. (2009), to which we applied the same selection criteria as for the FORS2 observations. As this is then exactly the parent sample for the observations, it replicates our selection function. We base an estimate of the overdensity on this sample.

To better address the issue of incompleteness, we employ the UVISTA catalog from McCracken et al. (2012), containing in total 1747 objects in the zCOSMOS-deep field and with $z_{\rm phot}$ (Ilbert et al. 2013) consistent with the protocluster redshift. This sample is K-selected and complete (to 95%) down to

$K_{AB} = 23.8$, corresponding to an approximate mass completeness limit of $\sim 10^{10}\,M_{\odot}$. We include this sample to look for differences in the galaxy population at the protocluster position with respect to the field. As we are only interested in differential effects, it is acceptable if our sample is not complete toward lower masses as long as it includes the objects we are interested in. It should, however, be noted that the UVISTA sample does not necessarily include the known spectroscopic members (in fact, it only contains 6 of the 11 members).

4.2. Overdensity

We can roughly estimate the overdensity of the protocluster by using the parent photometric sample from which we selected the targets for observation.

To that end, we calculate the field density in the $0.^{\circ}6 \times 0.^{\circ}62$ zCOSMOS-deep (densely sampled) area within the redshift range $z_{\rm cl} \pm 0.12$, which corresponds to $\pm 10{,}000\,{\rm km\,s^{-1}}$, to encompass the photo-z uncertainty. Then $\rho_{\rm field} = \frac{N_{\rm field}}{1/3 \times {\rm area} \times (l^3_{\rm max} - l^3_{\rm min})}$, where l denotes the comoving distance along the line of sight, and $l_{\rm min}$ and $l_{\rm max}$ correspond to the distance at $z_{\rm cl} - 0.12$ and $z_{\rm cl} + 0.12$. The "area" is the area of zCOSMOS-deep ($1.13 \times 10^{-4}\,{\rm sr}^2$).

When computing the density of the protocluster, we correct for the effect of the redshift uncertainty. The $\Delta v \pm 700\,{\rm km\,s^{-1}}$ of the spectroscopic members presumably overestimates the extent of the protocluster along the line of sight. We therefore assume that in reality the excess of objects concentrates within the $r_{\rm phys} = 1.4\,{\rm Mpc}$ radius, both along the line of sight and radially. Hence, the density of the protocluster is as follows: $\rho_{\rm cl} = \frac{11}{\pi r^2_{\rm com}\, l_{\rm com}}$, with $r_{\rm com} = r^{*}_{\rm phys}(1 + z_{\rm cl})$ and $l_{\rm com} = 2{*}r_{\rm com}$. Then the overdensity is given by $\delta = (\rho_{\rm cl} - \rho_{field)}/\rho_{\rm field} = 10$.

We double-checked our assumption of the spectroscopic members being concentrated within a radius of 1.4 pMpc = 4.8 cMpc. To that end, we determined the spread in the cosmological redshifts of the 16 mock protoclusters (being a measure for the "true" distribution of the protocluster member galaxies). The average rms of these redshifts is 0.006, translating to 7.3 cMpc, which is consistent with the 4.8 cMpc radius from above, suggesting that our assumption was valid but that we may slightly overestimate the overdensity.

An overdensity of 10 implies, in line with the simulations, that while the protocluster is not likely to be gravitationally bound yet, it has made its turnaround.

4.3. Radio Galaxies

Whereas this protocluster has been selected purely through a FOF approach on a spectroscopic sample, it is well established that radio galaxies are beacons for high-z overdensities (see for example Miley et al. 2006; Hatch et al. 2011; and others). We searched the publicly available FIRST catalog (White et al. 1997) for sources at the protocluster position and found a radio galaxy at (R.A. = 150.0025, dec1. = 2.2586) with a flux of 4.21 mJy. This position coincides with the protocluster with an offset of 0.5 pMpc from the center. Castignani et al. (2014) also report a structure at $z = 2.39$ at our protocluster position, identified with a Poisson probability method using photometric redshifts looking for overdensities around radio galaxies. They associate their structure with the same radio galaxy and quote a photometric redshift of $z_{\rm phot} = 2.2 \pm^{0.32}_{0.44}$ for it. Given the uncertainty in photometric redshifts, it is possible that our protocluster and the structure from Castignani et al. are the same overdensity and associated with the FIRST radio galaxy. Without spectroscopy, however, we cannot make a decisive statement.

4.4. Does Environment Matter?

As discussed in the introduction, previous work finds at times contradictory results regarding environmental differentiation in protoclusters. The protocluster presented in this work has originally been selected from a sample of blue star-forming galaxies, as opposed to the predominantly Hα-selected samples of the aforementioned studies. This opens the door for the search for environmental signatures both identical and different.

To this end, we search for any differences in the masses, star formation rates, and the quiescent fraction in the protocluster. Because of our blue selection, we are, however, biased toward lower-mass and star-forming galaxies. To overcome this limitation, we rely on the UVISTA catalog described in Section 4.1.

We determine the fraction of massive ($M > 10^{10.5}\,M_{\odot}$) galaxies, as well as the fraction of highly star-forming (${\rm SFR} > 50\,{\rm M_{\odot}\,yr^{-1}}$) galaxies within the protocluster, consistent with the proposed scenarios of either overabundance of massive galaxies (Hatch et al. 2011) or elevated star formation (Shimakawa et al. 2014). At the same time we also search for a difference in the quiescent fraction in comparison to the field, akin to low-redshift results.

We make use of the masses and SFRs that are given in the catalog and that are determined by the mass (SFR) of the best-fitting template defined by the median of the likelihood distribution from the photo-z fitting procedure. The selection of quiescent galaxies is also taken from UVISTA, where they employ a criterion based on NUV-*R*/*R*-*J* colors. In total, 73 galaxies with $z_{\rm phot}$ consistent with the protocluster redshift are flagged as quiescent.

We calculate the respective fractions of massive, star-forming, and quiescent galaxies in the protocluster in a cylinder of $r = 1.4\,{\rm Mpc}$ radius (physical, the protocluster radius) and a length of $\pm 10{,}000\,{\rm km\,s^{-1}}$ (to encompass the photo-z uncertainty). To compute the field values, we put down cylinders of the same volume at 100 random positions in the zCOSMOS-deep field.

Figure 5 shows these fractions in comparison with the field: the fraction of massive galaxies on the left, the fraction of star-forming galaxies in the middle, and the quiescent fraction on the right. While we see a trend toward slightly more massive and quiescent galaxies within the protocluster, this is not statistically significant within our sample. Despite its likely evolution into a very massive $z = 0$ cluster, we do not see evidence for environmental differentiation at this stage, although it is possible that a weak effect was not detected because of the large errors caused by the use of photo-z.

5. SUMMARY AND CONCLUSIONS

We presented a $z = 2.45$ protocluster with 11 spectroscopically confirmed members. It was first identified in zCOSMOS-deep and then followed up with FORS2 spectroscopy. Its member galaxies lie within a radius of 1.4 Mpc (physical) on the sky and within $\Delta v = \pm 700\,{\rm km\,s^{-1}}$. We estimated an overdensity of 10, in line with the structure having

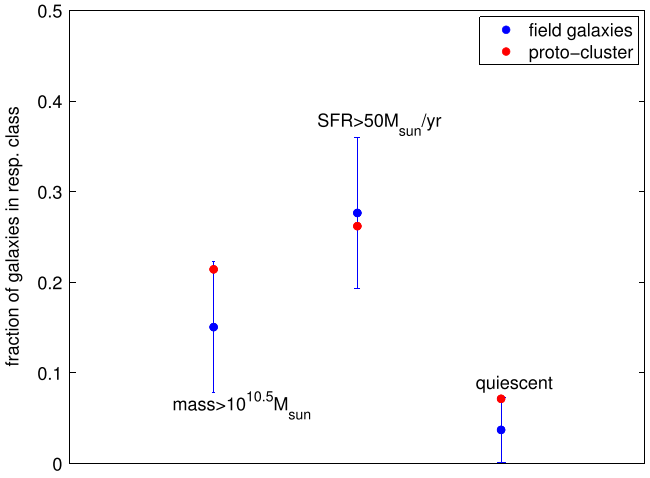

Figure 5. Fraction of massive $M > 10^{10.5}\,M_{\odot}$ (left), highly star-forming SFR $> 50\,M_{\odot}\,\mathrm{yr}^{-1}$ (middle), and quiescent galaxies in the protocluster (red) and in the field (blue). There is a weak trend for more massive and quiescent galaxies within the protocluster; this is, however, not significant.

made the turnaround but not having accreted its member galaxies onto a common DM halo.

This picture is confirmed by comparison of the protocluster to similar structures in simulations. To that end, we carefully constructed mock catalogs that resemble the observational situation and identified analogous protoclusters therein. We follow the evolution of these mock protoclusters from $z \sim 2.5$ to $z = 0$. We find that indeed most of the member galaxies are still centrals in their own DM halo at $z \sim 2.5$. By $z = 0$ most of them share the same halo and hence form a cluster. Furthermore, the $z = 0$ halo is of $M \gtrsim 10^{14}$–$10^{15}\,M_{\odot}\,h^{-1}$, equivalent to a Virgo- or Coma-like cluster.

We identified all $z \sim 2.5$ mock progenitor galaxies that will by $z = 0$ share the DM halo with the originally identified mock protocluster galaxies. These galaxies would mostly be too faint for observations, but they still lie within the Δv ± 700 km s^{-1} to be associated with the protocluster. For each of the mock protoclusters there exist several hundred to thousands of these progenitors spread over an area with a diameter between 3 and 20 pMpc, and hence they occupy a much wider field than suggested by the originally identified members. This optical selection of protoclusters results, therefore, mostly in loose structures and a rich diversity of objects. In order to fully characterize the progenitor population of today's massive clusters, these wide fields need to be observed. The numbers from above furthermore hint at an extended structure in the zCOSMOS field.

In the last section, we studied the galaxy population in the area of the protocluster in the search for early signatures of environmental differentiation. We compared the fraction of massive, highly star-forming, or quiescent galaxies in the protocluster to the field. While we see a weak trend for more massive and quiescent galaxies in the protocluster, this is not statistically significant.

This research has been supported by the Swiss National Science Foundation (SNF) and the European Southern Observatory (ESO). It is based on observations undertaken at the ESO Very Large Telescope (VLT) under Program 290.A-5160(A). It also uses data products from observations made with ESO Telescopes at the La Silla Paranal Observatory under ESO program ID 179.A-2005 and data products produced by TERAPIX and the Cambridge Astronomy Survey Unit on behalf of the UltraVISTA consortium. The Millennium simulation databases used in this paper and the Web application providing online access to them were constructed as part of the activities of the German Astrophysical Virtual Observatory.

REFERENCES

Abadi, M. G., Moore, B., & Bower, R. G. 1999, MNRAS, 308, 947
Balogh, M., Eke, V., Miller, C., et al. 2004, MNRAS, 348, 1355
Behroozi, P. S., Wechsler, R. H., & Conroy, C. 2013, ApJL, 762, L31
Birrer, S., Lilly, S. J., Amara, A., Paranjape, A., & Refregier, A. 2014, ApJ, 793, 12
Capak, P., Aussel, H., Ajiki, M., et al. 2007, ApJS, 172, 99
Castignani, G. 2014, ApJ, 792, 114
Cooke, E. A., Hatch, N. A., Muldrew, S. I., Rigby, E. E., & Kurk, J. D. 2014, MNRAS, 440, 3262
Cucciati, O., Zamorani, G., Lemaux, B., et al. 2014, A&A, 570, A16
Daddi, E., Cimatti, A., Renzini, A., et al. 2004, ApJ, 617, 746
Diener, C., Lilly, S. J., Knobel, C., et al. 2013, ApJ, 765, 109
Dressler, A. 1980, ApJ, 236, 351
Elvis, M., Civano, F., Vignali, C., et al. 2010, yCat, 218, 40158
Gerke, B. F., Newman, J. A., Faber, S. M., et al. 2007, MNRAS, 376, 1425
Gobat, R., Daddi, E., Onodera, M., et al. 2011, A&A, 526, A133
Gunn, J. E., & Gott, J. R. 1972, ApJ, 176, 1
Guo, Q., White, S. M. D., Boylan-Kolchin, M., et al. 2011, MNRAS, 413, 101
Hatch, N. A., DeBreuck, C., Galametz, A., et al. 2011, MNRAS, 410, 1537
Henriques, B. M. B., White, S. M. D., Lemson, G., et al. 2012, MNRAS, 421, 2904
Hilton, M., Lloyd-Davies, E., Stanford, S., et al. 2010, ApJ, 718, 133
Ilbert, O., Capak, P., Salvato, M., et al. 2009, ApJ, 690, 1236
Ilbert, O., McCracken, H. J., LeFevre, O., et al. 2013, A&A, 556A, 55
Kawata, D., & Mulchaey, J. S. 2008, ApJ, 672, L103
Kitzbichler, M. G., & White, S. D. M. 2007, MNRAS, 376, 2
Knobel, C., Lilly, S. J., Kovač, K., et al. 2013, ApJ, 769, 24
Knobel, C., Lilly, S. J., Woo, J., & Kovač, K. 2014, arXiv:1408.2553
Kodama, T., Tanaka, I., Kajisawa, M., et al. 2007, MNRAS, 377, 1717
Kovač, K., Lilly, S. J., Knobel, C., et al. 2014, MNRAS, 438, 717
Koyama, Y., Kodama, T., Tadaki, K., et al. 2014, ApJ, 789, 18
Larson, R. B., Tinsley, B. M., & Caldwell, C. N. 1980, ApJ, 237, 692
Lemaux, B. C., Cucciati, O., Tasca, L. A. M., et al. 2014, A&A, 572, 41
Lemson, G., & the Virgo Consortium 2006, arXiv:astro-ph/0608019
Lilly, S. J., Le Brun, V., Maier, C., et al. 2009, ApJS, 184, 218
Lilly, S. J., Le Fevre, O., Renzini, A., et al. 2007, ApJS, 172, 7
Lilly, S. J., Peng, Y., Carollo, M., & Renzini, A. 2013, in IAU Symp. 295 The Intriguing Life of Massive Galaxies, ed. D. Thomas, A. Pasquali, & I. Ferreras (Cambridge: Cambridge Univ. Press), 141
Mainieri, V., Hasinger, G., Cappelluti, N., et al. 2008, yCat, 217, 20368
McCracken, H. J., Milvang-Jensen, B., Dunlop, J., et al. 2012, A&A, 544, A156
Miley, G. K., Overzier, R. A., Zirm, A. W., et al. 2006, ApJL, 650, L29
Moore, B., Katz, N., Lake, G., Dressler, A., & Oemler, A. 1996, Natur, 379, 613
Oemler, A., Jr. 1974, ApJ, 194, 1
Papovich, C., Momcheva, I., Willmer, C. N. A., et al. 2010, ApJ, 716, 1503
Pasquali, A., Gallazzi, A., Fontanot, F., et al. 2010, MNRAS, 407, 937
Peng, Y., Lilly, S. J., Kovač, K., et al. 2010, ApJ, 721, 193
Peng, Y., Lilly, S. J., Renzini, A., & Carollo, M. 2012, ApJ, 757, 4
Schinnerer, E., Sargent, M. T., Bondi, M., et al. 2010, ApJS, 188, 384
Shimakawa, R., Kodama, T., Tadaki, K., et al. 2014, MNRAS, 441, L1
Springel, V., White, S. D. M., Jenkins, A., et al. 2005, Natur, 435, 629
Steidel, C. C., Adelberger, K., Barmby, P., et al. 2005, ApJ, 626, 44
Steidel, C. C., Shapley, A. E., Pettini, M., et al. 2004, ApJ, 604, 534
Tanaka, M., Finoguenov, A., Ueda, Y., et al. 2010, ApJL, 716, L152
Tran, K., Papovich, C., Saintongue, A., et al. 2010, ApJ, 719, 126
van den Bosch, F. C., Aquino, D., Yang, X., et al. 2008, MNRAS, 387, 79
Venemans, B. P., Rottgering, H. J. A., Miley, G. K., et al. 2007, A&A, 461, 823
Weinmann, S. M., Kauffmann, G., van den Bosch, F. C., et al. 2009, MNRAS, 394, 1213
Wetzel, A. R., Tinker, J. L., Conroy, C., & van den Bosch, F. C. 2013, MNRAS, 432, 336
White, R. L., Becker, R. H., Helfand, D. J., Gregg, M. D., et al. 1997, ApJ, 475, 479
Wuyts, S., Foerster Schreiber, N. M., van der Wel, A., et al. 2011, ApJ, 742, 96